Cucurbit[7]uril Enhances Distance Measurements of Spin-Labeled Proteins.

Zhimin Yang, † Richard A. Stein, ‡ Maren Pink, $^{*,\perp}$ Peter Madzelan, $^{\parallel}$ Thacien Ngendahimana, $^{\$}$ Suchada Rajca, † Mark A. Wilson, $^{*,\parallel}$ Sandra S. Eaton, $^{*,\$}$ Gareth R. Eaton, $^{\$}$ Hassane S. Mchaourab, *,‡ and Andrzej Rajca *,†

†Department of Chemistry, University of Nebraska, Lincoln, Nebraska 68588-0304, United States.

[‡]Department of Molecular Physiology and Biophysics, Vanderbilt University, Nashville, Tennessee 37232, United States.

¹IUMSC, Department of Chemistry, Indiana University, Bloomington, Indiana 47405-7102, United States.

Department of Biochemistry and Redox Biology Center, University of Nebraska, Lincoln, Nebraska 68588-0304, United States.

§Department of Chemistry and Biochemistry, University of Denver, Denver, Colorado 80208, United States.

KEYWORDS. Host-guest systems • Cucurbiturils • EPR spectroscopy • Biophysics • Organic Radicals

ABSTRACT: We report complex formation between the chloroacetamide 2,6-diazaadamantane nitroxide radical (CIA-DZD) and cucurbit[7]uril (CB-7), for which the association constant in water, $K_a = 1.9 \times 10^6 \, \text{M}^{-1}$, is at least one order of magnitude higher than the previously studied organic radicals. The radical is highly immobilized by CB-7, as indicated by the increase of the rotational correlation time, τ_{rot} , by a factor of 36, relative to that in the buffer solution. The X-ray structure of CIA-DZD@CB-7 shows the encapsulated DZD guest inside the undistorted CB-7 host, with the pendant group protruding outside. Upon addition of CB-7 to T4 Lysozyme (T4L) doubly spin-labeled with the iodoacetamide derivative of DZD, we observe the increase in τ_{rot} and electron spin coherence time, T_{m} , along with the narrowing of inter-spin distance distributions. Sensitivity of the DEER measurements at 83 K increases by a factor 4 – 9, compared to the common spin label such as MTSL, which is not affected by CB-7. Inter-spin distances of 3-nm could be reliably measured in water/glycerol up to temperatures near the glass transition/melting temperature of the matrix at 200 K, thus bringing us closer to the goal of supramolecular recognition-enabled long-distance DEER measurements at near physiological temperatures. The X-ray structure of DZD-T4L 65 at 1.12 Å resolution allows for unambiguous modeling of the DZD label (0.88 occupancy), indicating undisturbed structure and conformation of the protein.

INTRODUCTION

Tremendous efforts have been made to probe macromolecules in natural biological systems that would provide insight into their structures and functions. Site-directed spin labeling (SDSL) pulsed electron paramagnetic resonance (EPR) dipolar spectroscopy (PDS), which includes double electron–electron resonance (DEER) and double quantum coherence (DQC), is among the best techniques for accurate measurement of the conformations of flexible regions of biomolecules. The advantages include high sensitivity, wide dynamic range, absolute distance distributions, and minimal structural perturbation

from relatively small-size nitroxide spin labels.^{2,3} The most widely used spin label for SDSL is methane thiosulfonate pyrroline nitroxide (MTSL),¹¹ which selectively binds to cysteine, that can be introduced at selected locations by mutagenesis to provide doubly-labeled proteins.^{1,2} Using nitroxides, these measurements require cryogenic temperatures because of the dynamic averaging effects associated with methyl group rotation, which shorten the electron spin coherence time ($T_{\rm m}$) between about 80 and 300 K.¹²⁻¹⁵

Efforts have long been made with limited success to raise the experimental temperature range for the measurements.

A promising approach to DQC distance measurements in the physiological temperature range was demonstrated using a spin label based on a carbon-centered trityl radical and immobilized T4 lysozyme (T4L) or nucleic acids. 16,17 The inherent disadvantage of the trityl label is the lengthy synthesis, physical size, and hydrophobicity, and the distances can only be measured by the less commonly available DQC method,4,18,19 because the spectral width, even at Q-band, is too narrow for DEER, unless the trityl label is ¹³C substituted.^{20,21} Distance measurement up to 4 and 5 nm at physiological temperature was demonstrated by saturation recovery EPR spectroscopy of protein labeled with a nitroxide or a trityl spin label which have long electron spin-lattice relaxation times (T_1) and fast relaxing metal ion, such as Cu²⁺.²²⁻²⁴ Notably, the experiment requires insertion of the 5-residue, GGGHG, Cu²⁺⁻binding loop into the protein sequence.

We have developed a new generation of nitroxide spin labels devoid of methyl groups around the N-O moiety, such as IA-Spiro²⁵ and a compact iodoacetamide diazaadamantane (IA-DZD) spin label (Figure 1),²⁶ that can provide DEER measurements with improved sensitivity. T4L doubly spin-labeled with IA-DZD possesses sufficiently long $T_{\rm m}$ to allow for measurement of distances of up to 4 – 5 nm at 150 K and, with a sensitivity that is superior to MTSL, at 80 K.

Figure 1. Structures of spin labels, model nitroxide ClA-DZD, and dicationic nitroxide bPTO.

Adamantane and its derivatives are a notable family of molecular guests for supramolecular complexation with macrocyclic cages. We were enticed by the strong affinity of adamantane and intrigued to explore the possibility of employing supramolecular chemistry to facilitate long-distance DEER measurements at near physiological temperatures. We have examined the host-guest supramolecular complexation of IA-DZD and β -cyclodextrin (β -CD), in which we observed the slightly elongated T_m that further enhanced the sensitivity of DEER distance measurements. 26 These results inspire us to pursue further extraordinary supramolecular hosts for superior complexation with adamantane nitroxides.

Cucurbit[n]urils (CB-n) is a family of macrocyclic cages with exceptional recognition properties in aqueous medium that have been widely investigated for its applications in drug delivery system and advanced functional materials.^{27,28}

Among the CB-n (n = 6 - 8) family, CB-7 is the most water soluble host and has the strongest association constants, K_a = $7.2 \times 10^{17} \, \text{M}^{-1}$ in D_2O , with selected diamagnetic dicationic guests.²⁹⁻³¹ However, nitroxides as guests are far behind,³²⁻ ³⁴ with the reports of strongest $K_a \approx 2 \times 10^5 \,\mathrm{M}^{-1}$ for dicationic nitroxide radical **bPTO** (Figure 1)³⁵ and $K_a = 2.8 \times 10^6 \text{ M}^{-1}$ for a TEMPO-cobaltocenium derivative, based on inclusion of cobaltocenium moiety within CB-7.36 Nevertheless, the typical association constants for neutral adamantane derivatives with CB-7 are several orders magnitude higher than those with β -CD,^{27,37} thus much tighter complexes with superb association constant may be expected for the DZD nitroxide and CB-7 than for β -CD. Thus, we envisage narrow distance distributions and improved sensitivity of DEER distance measurement for the spin labeled DZD-T4L in the presence of CB-7, when the spin labels are at solvent exposed sites.

Herein we report the complex formation between the diazaadamantane nitroxide radical (DZD) and CB-7, for which the association constant in water is at least one order of magnitude higher than for previously studied organic radicals. The complexed DZD is highly immobilized by CB-7, as indicated by the increase of the rotational correlation time (τ_{rot}) by a factor of 36, compared to that in buffer solution. The X-ray structure of the ClA-DZD@CB-7 complex clearly shows the encapsulated DZD guest inside the undistorted CB-7 host, with the pendant group protruding outside. Addition of CB-7 to T4L doubly spin-labeled with IA-DZD (DZD-T4L) increases both the $\tau_{\rm rot}$ of the DZD spin label and its electron spin coherence time, $T_{\rm m}$, and importantly, narrows the inter-spin distance distributions. Sensitivity of the DEER measurements at 83 K increases by a factor 4 – 9, compared to the common spin label such as MTSL, which is not affected by CB-7. In addition, inter-spin distances of 3-nm could be reliably measured in glycerol/water up to a temperature of 200 K, which is near the glass transition/melting temperature of the matrix, thus bringing us closer to the goal of supramolecular recognition-enabled long-distance DEER measurements at near physiological temperatures. We also report the crystallographic characterization of DZD-T4L 65 at 1.12 Å resolution that allows for unambiguous modeling of the DZD label (0.88 occupancy) to illustrate that the DZD label leaves intact both structure and conformation of the protein. These results are advances in the supramolecular approach to the DEER distance measurements and lay a foundation for potential applications to probe macromolecules in natural biological systems at physiological temperatures.

RESULTS AND DISCUSSION

- **1. Complexation of CIA-DZD with CB-7.** Our objective is to explore the extent of CB-7 complexation with DZD spin labeled protein to gain insight into the potential benefit of supramolecular recognition in DEER distance measurements. CIA-DZD, which is a synthetic precursor to IA-DZD, 26 is less hydrophobic than IA-DZD, and thus it is expected to resemble the DZD-linked-to-Cvs on protein.
- 1.1. Isothermal calorimetry (ITC). Nitroxide radical CIA-DZD shows the highest association constant, $K_a = 1.9 \times 10^6 \,\mathrm{M}^{-1}$, in water among supramolecular complexes of neutral and

charged nitroxide radicals with CB-7 (Table 1). 35,38 Notably, this value of K_a is larger by a factor of 2500, compared to that previously reported for the ClA-DZD@ β -CD complex, 26 affirming the superior binding between DZD and CB-7.

In phosphate buffer containing 69 mM Na⁺, we observe K_a = 3.4×10^6 M⁻¹, which is 75% higher than that in pure water. The increase in K_a might suggest *cooperative binding* of sodium cations to the NO moiety of DZD in the complex.³⁹ Such binding may be facilitated by the relatively large partial negative charge on the oxygen atom of the highly pyramidal NO moiety of DZD nitroxide.²⁶ This observation is contrary to the reports of *competitive binding* of alkali metal cations with supramolecular guests,^{40,41} including nitroxide radicals.^{38,42} In buffer containing tris(hydroxymethyl)aminomethane (Tris) and 3-(*N*-morpholino)propane sulfonic acid (MOPS), K_a is lower than in water or phosphate buffer. For example, ITC measurements give K_a = 3.7×10^5 M⁻¹ in TrisMOPS 1, containing 53 mM Na⁺ and 9 mM MOPS, and K_a = 1.0×10^5 M⁻¹ in Tris buffer, without MOPS and Na⁺ (Table 1).

Table 1. Isothermal Calorimetry: Association Constants (K_a) of ClA-DZD with CB-7 and β-CD.

Host	Medium	Na+ (mM)	рН	$K_{\rm a} \times 10^5$ (M ⁻¹)
CB-7	water	0	~7	19.3 ± 0.8
	phosphatea	69	7.48	33.7 ± 1.1
	Tris-MOPS-1b	53	7.24	3.74 ± 0.07
	Tris-MOPS-2b	3	~7	0.432 ± 0.018
	Tris ^{b,c}	0	7.26	1.03±0.14
β-CD	water	0	~7	(7.55±0.07)×10 ⁻³

 $^{\rm a}$ 50 mM Phosphate. $^{\rm b}$ All 6 mM Tris buffers contain 0.01 mM EDTA; in addition, tris-MOPS-1 and -2 contain 9 mM MOPS, 3-(*N*-morpholino)propane-1-sulfonic acid and 0.02% (by weight) NaN₃; tris-MOPS-1 has 50 mM NaCl. $^{\rm c}$ pH is adjusted using 2.73 mM Tris and 3.27 mM Tris hydrochloride. Further details may be found in the SI: Table S4 and Figs. S7–S13.

1.2. X-ray crystallography. CB-7 has a propensity to form supramolecular gels in aqueous solution,^{43,44} and thus it is difficult to crystallize. However, there are numerous examples of crystalline inclusion complexes of CB-7 with neutral and cationic guests.⁴⁵⁻⁴⁷ Notably, to our knowledge, only a few single crystal X-ray structures of nitroxide (mostly TEMPO-like) complexes with CB-8 have been reported^{35,36,48-50} and there are only two reports on nitroxide (TEMPO-like and nitronyl nitroxide) complexes with CB-7.^{50,51}

Crystals of ClA-DZD@CB-7 complex are obtained by slow solvent evaporation from a 1:1 molar mixture of ClA-DZD and CB-7 in water. A complete set of X-ray diffraction data to a resolution of 0.84 Å is collected. The structure reveals the formation of a 1:1 complex of ClA-DZD with CB-7. The

presence of nitroxide radicals inside the CB-7 host is evidenced by the average N-O bond length of 1.296 Å (Table S2, SI), which is comparable to 1.2843(19) Å found in IA-DZD spin label.²⁶ The asymmetric unit consists of four independent ClA-DZD@CB-7 supramolecules and at least 41 molecules of co-crystallized water molecules. All the water molecules are positioned outside the CB-7 cavity, which is consistent with large value of K_a observed by ITC (Table 1). In one of the supramolecules, the CIA-DZD guest is not disordered; however, in the other three supramolecules, the host is disordered over two or three positions (Figs. S2 and S3, SI). As illustrated in Figure 2A&B, the ClA-DZD molecule is approximately placed at the center of the near-perfect 7fold symmetric host, suggesting a good size match between the guest and host. In contrast, in the X-ray structure of a TEMPO derivative, the CB-7 cavity is significantly distorted from 7-fold symmetry.⁵⁰ We find 10 close contacts ≤ sum of vdW radii, predominantly non-classical H-bonds, between the guest and the host (Fig. S2, SI); this is consistent with a near perfect fit of the DZD nitroxide with the CB-7 cavity. The pendant CIA-unit is exposed outside the portals of CB-7 (Figure 2B).

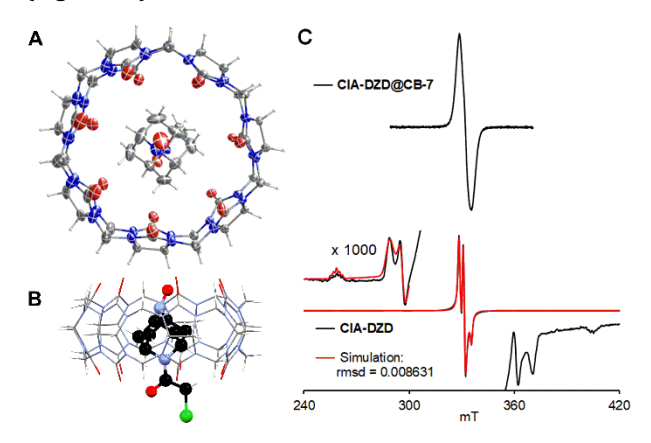


Figure 2. X-ray crystallography of ClA-DZD@CB-7 at 123 K: (A) top view, Ortep plot with carbon, nitrogen, oxygen, and chlorine atoms depicted with thermal ellipsoids set at the 50% probability level and (B) side view, the guest and host are shown in ball-and-stick and in wire plots. Molecules of water are omitted for clarity. (C) CW EPR spectra of polycrystalline ClA-DZD@CB-7 and ClA-DZD at room temperature. For more details, see: SI, Tables S2 and S3, and Figs. S2–S6.

We confirm the presence of nitroxide radicals in the crystals of ClA-DZD@CB-7 by EPR spectroscopy. The spectrum consists of a single peak (Figure 2C), which is broadened by unresolved magnetic dipole-dipole interactions, corresponding to inter-spin distances of about 13 Å (Fig. S6, SI). This result agrees with the nearest neighbor nitroxide-nitroxide distances in the X-ray structure, as illustrated by the 0···O contact range of 10-21 Å within the asymmetric unit. Notably, this spectrum is significantly different compared to that for polycrystalline ClA-DZD, which consists of well resolved center peaks for magnetically isolated $S=\frac{1}{2}$ radical crystal defects and the broader side-peaks (Figure 2C); the side-peaks correspond to S=1 thermally excited state for the dimer of nitroxides with nitroxide-nitroxide contacts of <2.6 Å.²⁶

1.3. CW EPR spectroscopy. We investigate complexation of ClA-DZD with CB-7 in Tris-MOPS-1 buffer (Table 1) by CW EPR spectroscopy (Figure 3).

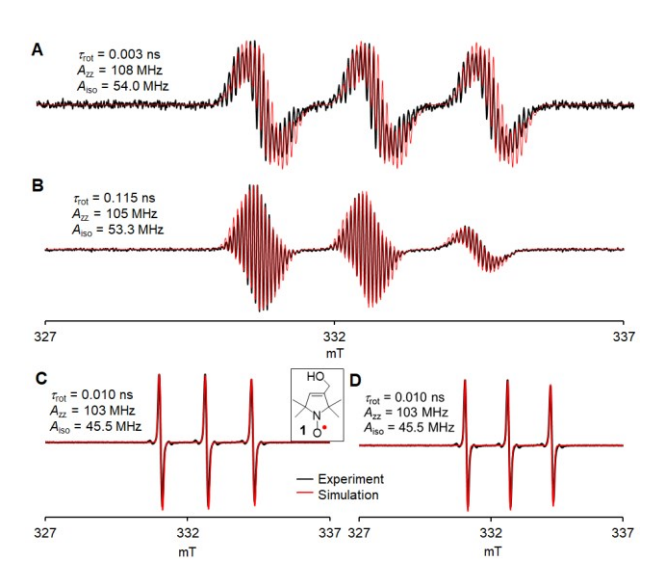


Figure 3. EPR spectroscopy in fluid Tris-MOPS-1 buffer (Table 1) at 295 K: rotational correlation times, $\tau_{\rm cor}$, and 14 N hyperfine tensor components, $A_{\rm zz}$, and isotropic 14 N hyperfine couplings, $A_{\rm iso}$, 52 (A) 0.28 mM ClA-DZD (B) 0.28 mM ClA-DZD with 2 equiv of CB-7; (C) 0.25 mM model pyrroline nitroxide 1; (D) 0.25 mM 1 with 2 equiv of CB-7. Enlarged version of this figure and a summary of fitting parameters may be found in the SI: Fig. S14 and Table S5.

We first acquire the EPR spectrum of 0.28 mM ClA-DZD to determine the ¹⁴N hyperfine coupling, $A_{\rm iso}$, and $\tau_{\rm rot}$. ⁵² Upon addition of 2 equiv of CB-7, the spectrum undergoes a dramatic change, with a small decrease of Aiso, from 54 to 53.3 MHz, and a large increase of $\tau_{\rm rot}$, by a factor of 36, from 0.003 to 0.115 ns. For comparison, we carry out the analogous experiment using pyrroline nitroxide 1 (a model compound for MTSL), from which we find that $A_{iso} = 45.5 \text{ MHz}$ and $\tau_{\rm rot}$ = 10 ps remain unchanged by addition of CB-7, indicating the absence of complexation by CB-7. The decrease in A_{iso} is expected upon inclusion of nitroxide radical into the hydrophobic cavity of CB-7.35,38,42,53,54 However, the formation of the ternary complex (see above, ITC) presumably impedes the decrease of Aiso. 35,38,39,42,50,53,54 Unlike all nitroxides studied for CB-7 or CB-8 complexation to date.35,38,42,50,53,54 ClA-DZD is a conformationally-fixed, relatively rigid radical, with much greater charge separation within the NO moiety as suggested by the greater magnitude of its $A_{\rm iso}$, 55 compared to typical nitroxides, including 1 (Figure 3). The rigidity and the increased charge separation in CIA-DZD might also contribute to the cooperativity in binding of Na+ to nitroxide@CB-7 complex, as observed in the ITC studies. The increase in $\tau_{\rm rot}$ and decrease in $A_{\rm zz}$ are analogous to what was observed when IA-DZD was complexed with β-CD.⁵⁶

2. Complexation of DZD-T4L with CB-7. Spin labeling of the T4L mutants is carried out using established methods as described in the Experimental section, to obtain DZD-T4L

135, DZD-T4L 65, and doubly labeled DZD-T4L 65/80 and DZD-T4L 65/135.

2.1. X-ray Crystallography of DZD-T4L 65. The crystals of DZD-T4L 65 were grown using established conditions as described in the Experimental section. The DZD label is attached through a chemically robust sulfide (S-C) linkage to the sole cysteine residue of the triple C54T/C97A/K65C T4L mutant, placing the label near the N-terminal portion of helix C, which connects the two domains of the enzyme (Figure 4A). Notably, DZD-T4L is structurally nearly identical to the unmodified protein, with a C_{α} RMSD of 0.34 Å to PDB 2LZM.⁵⁷

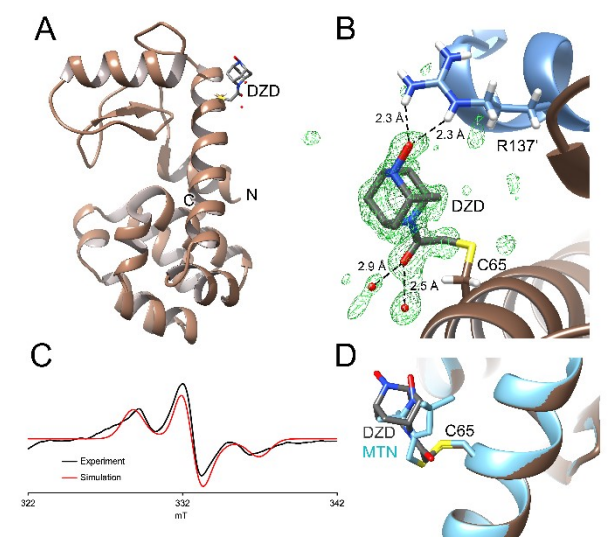


Figure 4. DZD-T4L 65: (A) The ribbon diagram of T4L showing the DZD label at C65 near the N-terminal region of helix C. (B) Minimally biased omit mF $_0$ -DF $_c$ electron density contoured at 3.0 σ (green) for the DZD label, which was calculated prior to the introduction of DZD into the structural model. Hydrogen bonds are shown as dotted lines with distances. R137 is from a neighboring molecule in the crystal lattice (blue, primed label) and makes a bifurcated hydrogen bond with the oxygen atom of the nitroxide label. (C) The CW EPR spectrum of polycrystal-line DZD-T4L in reservoir solution prior to X-ray data collection confirms the presence of the radical on the spin label (Fig. S1, SI). (D) A comparison of the DZD label (this work, gray) and the MTN spin label from PDB 6PGY, showing similar overall orientations in the crystal.

X-ray diffraction data were recorded to 1.12 Å resolution, allowing the DZD label to be modeled into unambiguous $mF_o\text{-}DF_c$ difference electron density extending from Cys65 (Figure 4B). The label occupancy is 0.88 as refined in PHE-NIX and its atomic displacement parameters (ADPs) are elevated (DZD, <ADP>=25.38 Ų), compared to neighboring atoms (Cys65 <ADP>=13.13 Ų), indicating some disorder of the label. Additional evidence for local disorder is the presence of some minor unmodeled difference density in the vicinity of the DZD moiety. Apart from the covalent attachment to Cys65, the label makes only one other direct contact with the protein: a bifurcated hydrogen bond⁵8 between the O1 atom of the label to the guanidinium group of Arg137 from a neighboring molecule in the lattice (Figure 4B). However, there are two hydrogen bonds between the

carbonyl oxygen atom (O2) of the DZD to nearby water molecules that provide indirect, solvent-mediated contacts between the label and the protein (Figure 4B). Because these contacts are predominantly with neighboring molecules in the lattice, it is likely that the DZD label has more orientational freedom when T4 lysozyme is in solution.

We attempted to both co-crystallize and soak CB-7 into DZD-T4L crystals without success. The crystal structure of DZD-T4L indicates that the CB-7 is too large to be accommodated in the crystal lattice at the Cys65 label site. These constraints are specific to this crystal lattice and are not expected to play a role in the solution behavior of CB-7-DZD-T4L complexes.

We determined the chemical species present at the N-O bond of the DZD label by unrestrained refinement and bond length analysis (see: Experimental). The N1-O1 bond length is 1.5806(611) Å after removing the distance restraint on this bond and inverting the least squares matrix in SHELXL. The PHENIX-refined model, which is the one deposited in the PDB, has a restrained N-O bond length of 1.54 Å. In both cases, this bond length is markedly longer than the expected N-O bond length for a nitroxide radical, which is 1,2843(19) Å in IA-DZD spin label.²⁶ Therefore, we conclude that the crystallized DZD label on T4L is likely the corresponding hydroxylamine. The DZD-T4L crystals initially contain some radical with the expected EPR features of DZD, indicating that the radical species survives crystallization (Figure 4C). One possible reason for conversion of the radical to the hydroxylamine in the crystal structure is X-ray radiation damage from the intense 17 keV synchrotron X-ray beam, although we did not test this.

T4L is an established protein system for characterizing spin labels and multiple crystal structures have been determined of different spin labeled forms of the enzyme. 59-64 Because the motivation for deploying spin labels in T4L is often to characterize the site-resolved conformational dynamics of the protein, the sites of attachment differ in these studies. Hubbell and coworkers used the same K65C mutation in helix C to attach an MTSL nitroxide spin label to T4L.59 Two crystal structures containing closely related S-(1-oxyl-2,2,5,5-tetramethyl-2,5-dihydro-1H-imidazol-4-yl) thanesulfonothioate (PDB 3K2R) and S-[(1-oxyl-2,2,5,5-tetramethyl-2,5-dihydro-1H-pyrrol-3-yl)methyl] methanesulfonothioate (PDB 6PGY) attached to Cys65 via a disulfide are available, although neither have associated publications yet. Overall, the orientation of these spin labels is similar to DZD (Figure 4D), although neither makes the hydrogen bond between the nitroxide oxygen atom to the symmetryrelated Arg137 residue that is observed in the present structure. Because of the absence of a stabilizing contact, the spin label-T4L tends to have more crystallographically disordered labels, with correspondingly weaker supporting electron density.

2.2. CW EPR spectroscopy. Analysis of the room temperature CW spectra of DZD-T4L 135, DZD-T4L 65, and doubly labeled DZD-T4L 65/80 in 2:1 buffer/glycerol (w/g) matrix, show that binding of the label to the protein increases $\tau_{\rm rot}$ to 1.33, 1.41, and 1.76, respectively (Table S5, Figs. S15-S17, SI). The position dependence of $\tau_{\rm rot}$ is attributed to different interactions with neighboring sidechains. Upon addition of

2 – 4 equiv of solid CB-7 changes in EPR spectra indicate increases in τ_{rot} to 1.62, 1,62, and 2.00 ns, respectively and smaller values of A_{zz} and A_{iso} (Table S5, Figs. S15–S18, SI). For DZD-T4L 65/80, A_{iso} = 55.7 MHz decreases to 53.3 MHz upon addition of CB-7 (Fig. S19, SI). The increases in τ_{rot} suggest greater steric interactions with neighboring protein sidechains for the bulkier CB-7 bound spin label than for the label alone. The significant decreases in A_{iso} suggest a more hydrophobic environment for nitroxide radical inside the CB-7 cavity, similar to what was observed for CIA-DZD binding to CB-7 (Figure 3, Table S5) or IA-DZD to β -CD. 26 In summary, these results reveal the strong host-guest molecular recognition of nitroxide in DZD-T4L by CB-7 in 2:1 w/g matrix.

2.3 Electron spin relaxation times. Binding to CB-7 causes a significant increase of the electron spin coherence time, $T_{\rm m}$, at 80 K and 150 K; e.g., for DZD-T4L/CB-7 at 80 K, $T_{\rm m}$ = 4.9 – 5.0 μs, compared to $T_{\rm m}$ = 4.4 – 4.5 μs for DZD-T4L/β-CD, $T_{\rm m}$ = 4.2 μs for DZD-T4L or IA-DZD, and $T_{\rm m}$ = 2.1 – 2.7 μs for MTSL (Table 2).

Table 2. Electron spin relaxation times: T_m and T_1 .^a

ъ.,		<i>m</i>	<i>m</i>	1	m	
Protein	spin label	T	$T_{\rm m}$	β	T_1	β
mutant		(K)	(µs)	·	(µs)	
/	MTSL	80	2.06	0.96	-	-
	MITOL	140	0.31	0.71	-	-
	IA-DZD	80	4.22	2.24	640	-
	IA-DZD	150	3.38	1.82	108	-
	IA DZD /CD Z	80	4.67	2.34	455	-
	IA-DZD/CB-7	150	3.72	1.70	100	-
		80	4.16	2.12	261	0.72
	DZD	80	4.46	2.14	320	0.71
		150	3.20	1.59	64	0.74
T4L 65/80		150	3.83	1.58	70	0.73
	D7D /CD 7	80	4.97	2.33	481	0.74
	DZD/CB-7	150	4.62	2.08	124	0.77
	D7D /0 CD	80	4.45	2.10	208	0.68
	DZD/β-CD	150	3.82	1.77	50	0.70
		80	4.20	2.03	218	0.70
	DZD	80	4.20	2.01	224	0.69
T4L 65/135	DZD	130	3.63	1.63	85	0.72
		150	3.24	1.50	76	0.70
	DED (CD 5	80	4.94	2.38	510	0.70
	DZD/CB-7	150	4.27	1.89	365	0.73
	D7D /0 CD	80	4.40	2.03	229	0.70
	DZD/β-CD	150	3.60	1.64	54	0.72

^aβ, exponential stretch parameter; data for β-CD²⁵ were re-fit with stretch exponential. Relaxation times are measured at the maximum amplitude peak in the echo-detected field-sweep spectra (Figs. S20 and S22, SI). T4L solutions contained 1 mM CB-7. MTSL data are obtained in trehalose/sucrose; in glycerol/water at 76 K, $T_{\rm m}$ = 2.7 μs is obtained. Uncertainties are >5% for $T_{\rm m}$ and about 10% for $T_{\rm L}$.

The exponential stretch parameter, β , increases upon complexation with CB-7, indicating enhanced immobilization of nitroxide. We note that T_1 at 80 K, increases from 200 – 300 μ s for DZD-T4L to 500 μ s for DZD-T4L/CB-7. Similar increases of T_1 , by a factor of 2 – 5 upon addition of CB-7, are found at 150 K (Table 2). The increase of T_1 limits the shot

repetition time, $>1.5*T_1$, for DEER experiments, resulting in slower data acquisition.

3. **DEER Distance Measurements.** The DEER distance measurements are carried out on the doubly labeled DZD-T4L and MTSL-T4L mutants 65/80 and 65/135 in a 2:1 w/g matrix without and with 1 mM CB-7 at 83 K. These two T4L mutants contain cysteines at solvent accessible sites that span C_{β} – C_{β} distances of 2.2 and 3.6 nm. Labeling efficiency of these mutants with IA-DZD is ca. 40% per cysteine, compared to ca. 70% with MTSL (Table S7, SI). Consequently, the expected modulation depth for DEER time traces is relatively lower for the DZD-labeled mutants.

Upon addition of CB-7 to the DZD-T4L mutants, significantly narrower main components of inter-spin distance distribution are observed, while the MTSL-T4L mutants are not affected by addition of CB-7 (Figure 5, Table 3). For both DZD-mutants at 83 K, we obtain the same widths (σ = 0.18 – 0.19, Table 3 and Table S8, SI) for the main components of the distance distribution with CB-7. Therefore, the CB-7 induced restriction of conformational freedom occurs to a similar extent in both mutants. The differential widths, broader for 65/135 compared to 65/80, of the unrestricted distributions (Table S8, SI) is most likely due to the higher mobility of the spin label at residue 135 compared to residues 80 or 65 (Figs. S15 – S17, SI). High mobility of MTSL at residue 135 in T4L was previously reported.

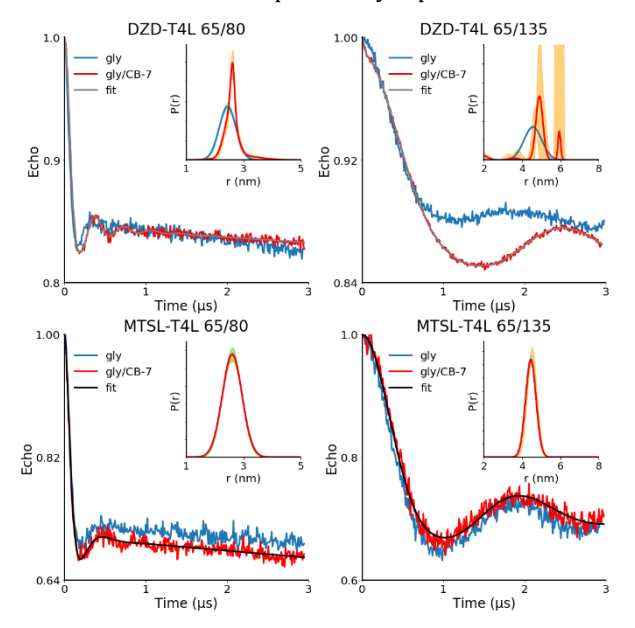


Figure 5. DEER distance measurements on doubly spin labeled DZD-T4L and MTSL-T4L in 2:1 w/g matrix without CB-7 (gly) and with 1 mM CB-7 (gly/CB-7) at 83 K. The water phase is Tris-MOPS-1 buffer (Table 1), i.e., 6 mM Tris, 9 mM MOPS, 0.01 mM EDTA, and 50 mM NaCl (pH 7.2). Main plots: normalized echo vs. time with fits, using a sum of Gaussians as the distance distribution. Inset plots: distance distributions with 95% confidence bands (orange lines). ⁶⁶ For additional details, including alternative distance distributions for DZD-T4L 65/135, see: SI, Tables S7 and S8, and Fig. S30 and S31.

As indicated by the limiting concentration (LC), defined as minimum concentration of spin label in the sample providing signal-to-noise ratio of 10 in one scan, sensitivity of the DEER measurements at 83 K in the presence of CB-7

increases by a factor 4 – 9 for DZD-T4L, compared to the MTSL-T4L. In addition, values of LC suggest that sensitivity of the measurements at T=83 K increases by a factor of 2.0 – 2.2 upon addition of CB-7 to the DZD-T4L mutants, while it remains approximately unchanged for the MTSL-T4L mutants (Table 3). This two-fold increase in sensitivity is attributed to the longer $T_{\rm m}$ observed in DZD-T4L mutants after addition of CB-7 (Table 2, Fig. S25-S26).

Table 3. DEER distance distributions and sensitivity measured at limiting concentration of spin label [LC].^a

		•				
d ₂ b (μs)	T4L	spin label	w/g matrix	T (K)	r (σ) [nm]	[LC] (μM)
3.5	65/80	DZD		83	2.44 (0.29)	6.48
			+ CB-7		2.56 (0.19)	3.28
		MTSL			2.60 (0.34)	14.5
			+ CB-7		2.60 (0.35)	12.9
	65/135	DZD			4.56 (0.47)	3.86
			+ CB-7		4.90 (0.19)	1.72
		MTSL			4.45 (0.27)	13.0
			+ CB-7		4.51 (0.26)	16.2
2.0	65/80	DZD	+ CB-7	83	2.62 (0.18)	0.57
				150	2.63 (0.26)	1.15
				170	2.58 (0.23)	1.78
				180	2.68 (0.69)	3.40
				190	2.61 (0.23)	12.2
1.2	65/80	DZD	+ CB-7	200	2.73 (0.49)	38.1

^a [LC] = $\{10^*[SL]^*(\#scans)^{1/2}\}/SNR$, where [SL] is concentration of spin label and SNR is signal-to-noise ratio. ^b d_2 = echo acquisition time. More details, including data for [LC] and β-CD,²⁶ may be found in the SI: Tables S8 and S9.

We explore further the highest possible temperature for practical DEER distance measurement (Figure 6). We use doubly spin labeled DZD-T4L 65/80 in a 2:1 w/g matrix with 1 mM CB-7, with aqueous phase corresponding to the 6 mM Tris buffer. We note that, for this DZD-T4L mutant in the presence of CB-7, $T_{\rm m}$ is only moderately decreased to 4.6 $\mu \rm s$ and $T_{\rm 1}$ is significantly decreased (by a factor of 4) to 120 $\mu \rm s$ at 150 K (vs. 80 K) (Table 2). These values of $T_{\rm m}$ and $T_{\rm 1}$ are perhaps slightly more favorable, compared to $T_{\rm m}=4.3$ $\mu \rm s$ and $T_{\rm 1}=175$ $\mu \rm s$ at 150 K for protein-bound perdeuterated, hydrophilic trityl spin label (mOX063-d₂₄). ¹⁹

The 2:1 water/glycerol matrix (v/v), corresponding to approximately 10 mol% glycerol in water, has been postulated to consist of mesoscopic domains of glycerol-rich (40 mol%) glass/liquid and water-rich ice cores in the temperature range 80–270 K. The glycerol rich domains possess a glass transition temperature, $T_{\rm g} \approx 170$ K, while the ice cores undergo a melting process in a broad range of temperatures, ca. 200 – 270 K. 67,68

Notably, we can observe DEER signal up to 200 K (Figure 6), which corresponds to the apparent onset of melting of water-rich ice cores in the 2:1 w/g matrix. To obtain a reasonable signal-to-noise ratio (SNR) in a reasonable amount of time at 200 K, we use a relatively short echo acquisition time, d_2 = 1.2 μ s and a short repetition time of 150 μ s, to reflect a shortened T_m and T_1 , respectively, at this temperature. No discernible signal was seen at higher temperatures.

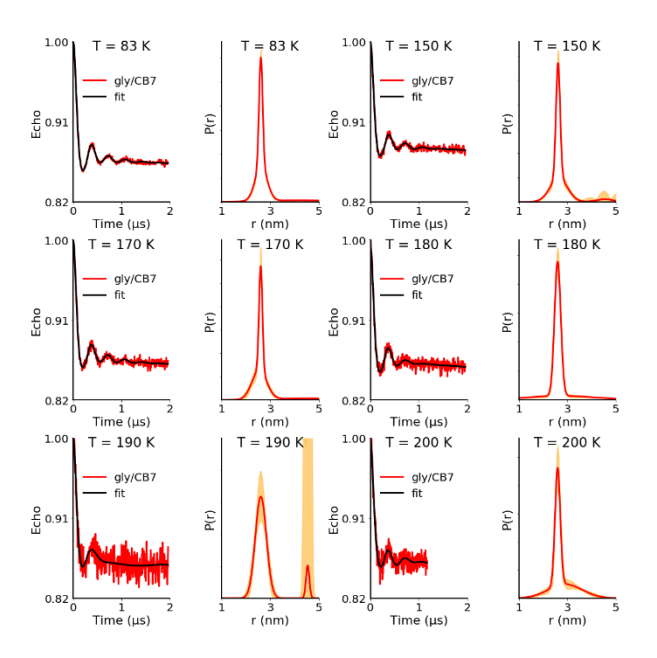


Figure 6. DEER distance measurements on doubly spin labeled DZD-T4L 65/80 in 2:1 w/g matrix with 1 mM CB-7 (gly/CB-7) at T=83-200 K: normalized echo vs. time with fits, using a sum of Gaussians, and distance distributions, P(r), with 95% confidence bands (orange lines).⁶⁶ The water phase is Tris-MOPS-1 buffer (Table 1). Additional information may be found in Table 3 and the SI: Table S9 and Fig. S32.

We note that such measurements at T=140-200 K would not be feasible on MTSL-T4L proteins, because of very small $T_{\rm m}=0.1-0.5$ µs, as determined for MTSL (Fig. S20, SI) or simple pyrroline nitroxide radical, such as 3-carbamoyl-2,2,5,5-tetramethyl-3-pyrrolin-1-oxyl.⁶⁹ We also note that MTSL-T4L 96 in 2:1 w/g matrix showed a discontinuity in the slope of the microwave power (P) saturation plots, ln $P_{1/2}$ vs 1/T, at $T\approx 200$ K;⁶⁹ this would suggest a significant change in electron spin relaxation times at that temperature. Further studies to understand changes in the microenvironment of nitroxide radicals, corresponding to

the abrupt disappearance of DEER signal at $210\ K$ will be needed.

CONCLUSION

The complex of neutral 2,6-diazaadamantane-based ClA-DZD nitroxide radical with CB-7 possesses the largest association constant to date among all studied nitroxides. The radical inside the host is significantly immobilized, as indicated by the increase of rotational correlation time by a factor of 36 upon complexation. The X-ray structure of the ClA-DZD@CB-7 complex shows the guest nitroxide radical encapsulated inside of the CB-7 host, with the ClA-side chain protruding outside of the host. This structure suggests that strong complexation of DZD nitroxide attached to protein by CB-7 is feasible. A strong host-guest molecular recognition, between CB-7 and DZD-based nitroxide radical, leads to substantial increase of the electron spin coherence time, $T_{\rm m}$, for DZD-T4L/CB-7 which is 4.9 – 5.0 μ s at 80 K and 4.3 – 4.6 μ s at 150 K. These relatively long $T_{\rm m}$ improve sensitivity of the DEER measurements at 83 K by a factor 4 - 9, compared to a common spin label such as MTSL, which is not affected by CB-7. In addition, a 3-nm distance may be reliably measured in aqueous buffer/glycerol up to a temperature of 200 K, which is near the glass transition/melting temperature of the matrix, thus bringing us closer to the goal of supramolecular recognition-enabled long-distance DEER measurements at near physiological temperatures. The X-ray structure of DZD-T4L 65 was obtained at 1.12 Å resolution, thus allowing for unambiguous modeling of the DZD label (0.88 occupancy). Most importantly, the presence of DZD label does not affect the structure and conformation of the protein.

EXPERIMENTAL SECTION

X-ray Crystallography.

CIA-DZD@CB-7: Crystals of CIA-DZD@CB-7 were obtained by slow evaporation of solvent from 1:1 molar solution of ClA-DZD and CB-7 in water. Data were collected at 123 K using Mo $K\alpha$ radiation and integrated (SAINT).⁷⁰ Intensity data were corrected for absorption using the Multi-Scan method (TWINABS).⁷¹ Space group P-1 was determined based on intensity statistics and the lack of systematic absences. The structure was solved with intrinsic methods and refined on F² using SHELX suite of programs.^{72,73} Crystal data for ClA-DZD@CB-7: C₄₂H₄₂N₂₈O₁₄, C₁₀H₁₄N₂₈ClN₂O₂, 10.25 H₂O, $M_r = 1577.38 \text{ g mol}^{-1}$, colorless block, 0.355 × $0.187 \times 0.096 \text{ mm}^3$, triclinic, P-1, a = 13.1522(12) Å, b = 13.1522(12) Å24.929(2) Å, c = 40.858(4) Å, V = 13282(2) Å³, Z = 8, $\mu(Mo)$ $K\alpha$) = 0.167 mm⁻¹, θ_{max} = 25.24°, 292,836 reflections measured, 54,462 independent ($R_{int} = 0.0967$), R1 = 0.1239 [I > $2\sigma(I)$], wR2 = 0.3413 (all data), residual density peaks: 1.420 and -1.062 e Å-3. Additional crystal and structure refinement data for CIA-DZD@CB-7 are in the Supporting Information and the file in CIF format, deposited to CCDC.

DZD-T4L 65: DZD-T4L 65 at 6.9 mg/mL in storage buffer (9 mM MOPS, 6 mM Tris pH 7.2, 0.1 mM EDTA, 50 mM NaCl, 0.02% sodium azide) was crystallized using sitting drop vapor equilibration by mixing 1 μ l of protein and 1 μ l of the

reservoir (1.6 M sodium/potassium phosphate pH 7.4, 100 mM NaCl, 40 mM β -mercaptoethanol) and incubating at room temperature for 3-10 days. This condition is commonly used for crystallization of T4 lysozyme. 57 Crystals measuring approximately 200x200x100 μm^3 in space group $P3_221$ were cryoprotected by transfer through light mineral oil (Fisher Scientific) until all surface mother liquor was removed and then cryocooled by immersion in liquid nitrogen.

X-ray diffraction data were collected at the Stanford Synchrotron Radiation Laboratory beamline 12-2 using 17 keV radiation, a Pilatus 6M pixel-array detector (PAD), and shutterless collection with 0.2 sec exposure per 0.15° oscillation at 85% beam attenuation. Data were processed with XDS,74 Pointless,⁷⁵ and Aimless⁷⁶ with final statistics provided in Table S1, SI. The initial model was obtained by molecular replacement in PHASER,77 using PDB 7LXA as a search molecule.⁷⁸ and then refined in PHENIX⁷⁹ using riding hydrogen atoms and anisotropic ADPs. Relative weights for both geometry and ADPs were optimized. Initial inspection of mF₀-DF_c electron density allowed unambiguous placement of the DZD label, which was subsequently refined using restraints generated in PRODRG.80 The model was manually improved in COOT81 between cycles of refinement and validated using tools in COOT,81 PHENIX,79 and MolProbity.82 Potassium and chloride ions were modeled in electron density where anomalous difference map peaks (>4 σ) and the local environment indicated probable ion identity. Anisotropic ADPs were validated using the PARVATI server.83 Crystallographic data and model statistics for DZD-T4L 65 are presented in Table S1, SI. The unrestrained length and estimated standard uncertainty (ESU) of the N-O bond of the DZD label was determined using SHELXL (version 2018/3),⁷³ as distributed in the CCP4 suite.⁸⁴ The converged PHENIX model was refined in SHELXL using a conjugate gradient least squares target function based on intensities (keyword HKLF 4). Riding hydrogen atoms and anisotropic ADPs were refined for the whole model and the SHELX version of the PRODRG restraints were used for the DZD label. Upon reaching convergence, the distance restraint (DFIX) on the N1-O1 bond was removed and the model was refined for an additional 20 cycles. The full least squares matrix on coordinates alone (i.e., the Hessian matrix excluding ADP elements) was inverted and ESUs determined by a final cycle of unrestrained refinement with full least squares (keywords L.S. and BLOC1) in SHELXL. Several crystals were transferred in the reservoir buffer into 3 quartz capillaries, sealed with capillary wax (Hampton Research cat # HR4-328) and used for EPR spectroscopy.

Complexation of ClA-DZD with CB7.

Isothermal titration calorimetry (ITC): association constants, K_a , and thermodynamic parameters for the formation of inclusion complexes of ClA-DZD were obtained from ITC (VP-ITC Microcal Inc., Northampton, MA). The experiments were carried out at 25 °C in a buffer or purified water as specified in Table 1. In a typical procedure, a degassed aliquot (1.42 mL) of 0.2 mM CB-7 solution was added to the reaction cell and an identical volume of solvent (buffer or water) without CB-7 was placed in the reference cell. A degassed 2.1 mM ClA-DZD solution (300 μ L) was

loaded in the titration syringe, and then added in 10 μL aliquots to the reaction cell under continuous stirring at 260 rpm. The titrant was injected over 12 s with an interval of 300 s between the injections. Typical ITC thermograms are provided in the SI, Figs. S7–S13.

EPR spectroscopy: CW EPR spectra were obtained on a Bruker EMX+ equipped with Bruker high-sensitivity cavity (Figures 2–4). (Field-swept echo detected spectra were obtained as described below.) The CW spectra were simulated with EasySpin, using either *pepper* or *chili* modules.⁵² More details may be found in the SI.

Spin labeling of T4L.

Sample labeling was carried out as previously described. 26,65,85 Briefly, T4L mutants were expressed in K38 cells in Luria Broth (LB) and purified using cation exchange chromatography. Labeling of the mutants was initiated by adding an excess of spin-label and incubating for 2 hours at room temperature, a second addition of spin-label was made and the samples incubated overnight at 4 °C. The samples were then desalted and concentrated.

Electron spin relaxation studies.

Field-swept echo detected spectra and relaxation times were recorded at X-band and Q-band on a Bruker E580 equipped with an Oxford ESR935 cryostat and a Bruker Xband ER4118X-MS5 split ring resonator or Q-band ER5107D2 resonator. The length of a $\pi/2$ pulse was 20 ns at X-band and 40 ns at Q-band. Field-swept echo-detected spectra were obtained with a two-pulse $\pi/2$ - τ - τ -echo sequence and 2-pulse phase cycling. The constant τ was 180 ns at X-band and 200 ns at Q-band. $T_{\rm m}$ was measured by two-pulse echo-decay with a $\pi/2$ - τ - τ -echo sequence and two-step phase cycling. T_1 was measured by inversion recovery with a π -T- π /2- τ - π - τ -echo sequence with variable T that is stepped to define the relaxation process. and twostep phase cycling. The constant τ in the inversion recovery pulse sequence was 200 ns at X-band and 360 ns at Q-band. Echo decays and inversion recovery curves were fitted with stretched exponentials (Table S6, Figs. S23, S24, S28).

DEER measurements.

The dipolar time evolution data was obtained at 83–200 K using a standard DEER four-pulse protocol, $(\pi/2)mw1-\tau1-(\pi)mw1-\tau1-(\pi)mw2-\tau2-(\pi)mw1-\tau2-echo,^{86}$ on a Bruker 580 pulsed EPR spectrometer operating at Q-band frequency (33.9 GHz). All pulses were square pulses with lengths of 12, 24, and 40 ns, for $(\pi/2)mw1$, $(\pi)mw1$, and $(\pi)mw2$, respectively. Temperature control was provided by an Oxford Instruments continuous flow cryostat controlled by an ITC503 temperature controller unit. Distance distributions were obtained from the time evolution data by assuming that the distance distribution can be approximated by a sum of Gaussians, 87,88 including Gaussian distance distributions with 95% confidence bands. 66

ASSOCIATED CONTENT

Supporting Information. This material is available free of charge via the Internet at http://pubs.acs.org.xxxxx

General procedures and materials and additional experimental details: Tables S1 – S9 and Figs. S1 – S32.

Accession Codes

Structure factors and coordinates for DZD-T4 lysozyme are available from the Protein Data Bank with accession code 8F11 (PDB id).

CCDC 2289150 contains the supplementary crystallographic data for this paper. These data can be obtained free of charge via www.ccdc.cam.ac.uk/data_request/cif, or by emailing data_request@ccdc.cam.ac.uk, or by contacting The Cambridge Crystallographic Data Centre, 12 Union Road, 495 Cambridge CB2 1EZ, UK; fax: +44 1223 336033...

AUTHOR INFORMATION

Corresponding Authors

- *Maren Pink, mpink@iu.edu
- *Mark Wilson, mwilson13@unl.edu
- *Sandra S. Eaton, sandra.eaton@du.edu
- *Hassane Mchaourab, hassane.mchaourab@Vanderbilt.Edu
- *Andrzej Rajca, arajca1@unl.edu

Present Addresses

^TZhimin Yang, Element Biosciences Inc., 10055 Barnes Canyon Rd, Suite 100, San Diego, CA 92121, USA.

Author Contributions

The manuscript was written through contributions of all authors. All authors have given approval to the final version of the manuscript.

Notes

Any additional relevant notes should be placed here.

ACKNOWLEDGMENT

We thank the National Institutes of Health (R01GM124310-01 to AR, SR, SSE, and HM) and National Science Foundation (CHE-1955349 and CHE-2247170 to AR) for support of this research. M.A.W. is supported by NIH R01GM139978. Support for the acquisition of the Bruker Venture D8 diffractometer through the Major Scientific Research Equipment Fund from the President of Indiana University and the Office of the Vice President for Research is gratefully acknowledged. Use of the Stanford Synchrotron Radiation Lightsource, SLAC National Accelerator Laboratory, is supported by the U.S. Department of Energy, Office of Science, Office of Basic Energy Sciences under Contract No. DE-AC02-76SF00515. The SSRL Structural Molecular Biology Program is supported by the DOE Office of Biological and Environmental Research, and by the National Institutes of Health, National Institute of General Medical Sciences (including P41GM103393). The contents of this publication are solely the responsibility of the authors and do not necessarily represent the official views of NIGMS or NIH. We thank Dr. Chan Shu (Nebraska) for obtaining EPR spectrum of DZD-T4L 65 crystals (Figure 4c) and reproducing selected ITC experiments.

REFERENCES

- Altenbach, C.; Marti, T.; Khorana, H. G.; Hubbell, W. L. Transmembrane Protein Structure: Spin Labeling of Bacteriorhodopsin Mutants. *Science* 1990, 248, 1088–1192. DOI: 10.1126/science.2160734.
- (2) Hubbell, W. L.; Lopez, C. J.; Altenbach, C.; Yang, Z. Technological Advances in Site-Directed Spin Labeling of Proteins. Current Opinion Structural Biology 2013, 23, 725–733.
- (3) Haugland, M. M.; Lovett, J. E.; Anderson, E. A. Advances in the Synthesis of Nitroxide Radicals for Use in Biomolecule Spin Labelling. *Chem. Soc. Rev.* 2018, 47, 668–680.
- (4) Jeschke G. DEER Distance Measurements on Proteins. *Ann. Rev. Phys. Chem.* **2012**, *63*, 419–446
- (5) Borbat, P. P.; Costa-Filho, A. J.; Earle, K. A.; Moscicki, J. K.; Freed, J. H. Electron spin resonance in studies of membranes and proteins. *Science* **2001**, *291*, 266–269.
- (6) Schmidt, T.; Wälti, M. A.; Baber, J. L.; Hustedt, E. J.; Clore, G. M. Long Distance Measurements up to 160 Å in the GroEL Tetradecamer Using Q-Band DEER EPR Spectroscopy. *Angew. Chem. Int. Ed.* 2016, 55, 15905–15909.
- (7) Dastvan, R.; Mishra, S.; Peskova, Y. B.; Nakamoto, R. K.; Mchaourab, H. S. Mechanism of Allosteric Modulation of P-Glycoprotein by Transport Substrates and Inhibitors. *Science* 2019, 364, 689–692.
- (8) Joseph, B.; Sikora, A.; Cafiso, D. S. Ligand Induced Conformational Changes of a Membrane Transporter in *E. coli* Cells Observed with DEER/PELDOR. *J. Am. Chem. Soc.* 2016, 138, 1844–1847.
- (9) Barth, K.; Hank, S.; Spindler, P. E.; Prisner, T. F.; Tampé, R.; Joseph, B. Conformational Coupling and *trans*-Inhibition in the Human Antigen Transporter Ortholog TmrAB Resolved with Dipolar EPR Spectroscopy. *J. Am. Chem. Soc.* 2018, 140, 4527–4533.
- (10) Jana, S.; Evans, E. G. B.; Jang, H. S.; Zhang, S.; Zhang, H.; Rajca, A.; Gordon, S. E.; Zagotta, W. N.; Stoll, S.; Mehl, R. A. Ultra-Fast Bioorthogonal Spin-Labeling and Distance Measurements in Mammalian Cells Using Small, Genetically Encoded Tetrazine Amino Acids. J. Am. Chem. Soc. 2023, 145, 14608–14620.
- (11) Berliner, L. J.; Grunwald, J.; Hankovszky, H. O.; Hideg, K. A Novel Reversible Thiol Specific Spin Label: Papain Active Site Labeling and Inhibition. *Anal. Biochem.* 1982, 119, 450–455.
- (12) Dzuba, S. A.; Maryasov, A. G.; Salikhov, K. M.; Tsvetkov, Yu. D. Superslow rotations of nitroxide radicals studied by pulse EPR spectroscopy. J. Magn. Reson. 1984, 58, 95–117.
- (13) Zecevic, A.; Eaton, G. R.; Eaton, S. S.; Lindgren, M. Dephasing of electron spin echoes for nitroxyl radicals in glassy solvents by non-methyl and methyl protons. *Mol. Phys.* **1998**, 95, 1255–1263.
- (14) Rajca, A.; Kathirvelu, V.; Roy, S. K.; Pink, M.; Rajca, S.; Sarkar, S.; Eaton, S. S.; Eaton, G. R. A Spirocyclohexyl Nitroxide Amino Acid Spin Label for Pulsed EPR Spectroscopy Distance Measurements. *Chem. Eur. J.* **2010**, *16*, 5778–5782.
- (15) Eggeling, A.; Soetbeer, J.; Fábregas-Ibáñez, L.; Klose, D.; Jeschke, G. Quantifying methyl tunneling induced (de)coherence of nitroxides in glassy *ortho*-terphenyl at low temperatures. *Phys. Chem. Chem. Phys.* 2023, 25, 11145–11157. DOI: https://doi.org/10.1039/D3CP01299A
- (16) Yang, Z.; Liu, Y.; Borbat, P.; Zweier, J. L.; Freed, J. H.; Hubbell, W. L. Pulsed ESR dipolar spectroscopy for distance measurements in immobilized spin labeled proteins in liquid solution. *J. Am. Chem. Soc.* **2012**, *134*, 9950–9952. DOI: https://doi.org/10.1021/ja303791p
- (17) Shevelev, G. Y.; Krumkacheva, O. A.; Lomzov, A. A.; Kuzhelev, A. A.; Rogozhnikova, O. Y.; Trukhin, D. V.; Troitskaya, T. I.; Tormyshev, V. M.; Fedin, M. V.; Pyshnyi, D. V.; Bagryanskaya,

details: Tables 51

- E. G. Physiological-temperature distance measurement in nucleic acid using triarylmethyl-based spin labels and pulsed dipolar EPR spectroscopy. *J. Am. Chem. Soc.* **2014**, *136*, 9874–9877. DOI: https://doi.org/10.1021/ja505122n
- (18) Borbat, P. P.; Mchaourab, H. S.; Freed, J. H. Protein structure determination using long-distance constraints from double-quantum coherence ESR: study of T4 lysozyme. *J. Am. Chem. Soc.* **2002**, *124*, 5304–5314. DOI: 10.1021/ja020040y
- (19) Hasanbasri, Z.; Singewald, K.; Gluth, T. D.; Driesschaert, B.; Saxena, S. Cleavage-Resistant Protein Labeling With Hydrophilic Trityl Enables Distance Measurements *In-Cell. J. Phys. Chem. B* 2021, 125, 5265–5274. DOI: https://doi.org/10.1021/acs.jpcb.1c02371
- (20) Poncelet, M.; Driesschaert, B. A ¹³C-Labeled triarylmethyl radical as an EPR spin probe highly sensitive to molecular tumbling. *Angew. Chem. Int. Ed.* 2020, *59*, 16451–16454. DOI: https://doi.org/10.1002/anie.202006591
- (21) Hasanbasri, Z.; Poncelet, M.; Hunter, H.; Driesschaert, B.; Saxena, S. A new ¹³C trityl-based spin label enables the use of DEER for distance measurements. *J. Magn. Res.* **2023**, *347*, 107363-1-8. DOI: https://doi.org/10.1016/j.jmr.2022.107363
- (22) Jun, S.; Becker, J. S.; Yonkunas, M.; Coalson, R.; Saxena, S. Unfolding of alanine-based peptides using electron spin resonance distance measurements. *Biochemistry.* 2006, 45, 11666–11673.
- (23) Yang, Z.; Jiménez-Osés, G.; López, C. J.; Bridges, M. D.; Houk, K. N.; Hubbell, W. L. Long-range distance measurements in proteins at physiological temperatures using saturation recovery EPR spectroscopy. J. Am. Chem. Soc. 2014, 136, 15356–15365.
- (24) Yang, Z.; Bridges, M. D.; López, C. J.; Rogozhnikova, O. Y.; Trukhin, D. V.; Brooks, E. K.; Tormyshev, V.; Halpern, H. J.; Hubbell, W. L. A triarylmethyl spin label for long-range distance measurement at physiological temperatures using T₁ relaxation enhancement. *J. Magn. Reson.* 2016, 269, 50–54. DOI: https://doi.org/10.1016/j.jmr.2016.05.006
- (25) Meyer, V.; Swanson, M. A.; Clouston, L. J.; Boratyński, P. J.; Stein, R. A.; Mchaourab, H. S.; Rajca, A.; Eaton, S. S.; Eaton, G. R. Room-temperature distance measurements of immobilized spin-labeled protein by DEER/PELDOR. *Biophys. J.* 2015, 108, 1213–1219.
- (26) Yang, Z.; Stein, R. A.; Ngendahimana, T.; Pink, M.; Rajca, S.; Jeschke, G.; Eaton, S. S.; Eaton, G. R.; Mchaourab, H. S.; Rajca, A. Supramolecular Approach to Electron Paramagnetic Resonance Distance Measurement of Spin-Labeled Proteins. *J. Phys. Chem. B*, 2020, 124, 3291–3299.
- (27) Barrow, S. J.; Kasera, S.; Rowland, M. J.; del Barrio, J.; Scherman, O. A. Cucurbituril-Based Molecular Recognition. *Chem. Rev.* 2015, 115, 12320–12406. DOI: https://doi.org/10.1021/acs.chemrev.5b00341
- (28) Shetty, D.; Khedkar, J. K.; Park, K. M.; Kim, K. Can We Beat the Biotin-Avidin Pair? Cucurbit[7]uril-Based Ultrahigh Affinity Host-Guest Complexes and Their Applications. *Chem. Soc. Rev.* **2015**, *44*, 8747–8761. DOI: 10.1039/C5CS00631G
- (29) Cao, L.; Šekutor, M.; Zavalij, P. Y.; Mlinarić-Majerski, K.; Glaser, R.; Isaacs, L. Cucurbit[7]uril·Guest Pair with an Attomolar Dissociation Constant. *Angew. Chem. Int. Ed.* 2014, 53, 988–993. DOI: 10.1002/anie.201309635
- (30) Sigwalt, D.; Šekutor, M.; Cao, L.; Zavalij, P. Y.; Hostaš, J.; Ajani, H.; Hobza, P.; Mlinarić-Majerski, K.; Glaser, R.; Isaacs, L. Unraveling the Structure-Affinity Relationship between Cucurbit[n]urils (n = 7, 8) and Cationic Diamondoids. *J. Am. Chem. Soc.* 2017, 139, 3249–3258. DOI: 10.1021/jacs.7b00056
- (31) Liu, W.; Samanta, S. K.; Smith, B. D.; Isaacs, L. Synthetic Mimics of Biotin/(strept)avidin. Chem. Soc. Rev. 2017, 46, 2391– 2403. DOI: 10.1039/C7CS00011A
- (32) Ouari, O.; Bardelang, D. Nitroxide Radicals with Cucurbit[n]urils and Other Cavitands. *Isr. J. Chem.* **2018**, *58*, 343–356.

- (33) Lucarini, M. Improving Spin Probe Methodologies to Investigate Supramolecular Assemblies. Eur. J. Org. Chem. 2020, 2995–3008.
- (34) Liu, F.; Karoui, H.; Rockenbauer, A.; Liu, S.; Ouari, O.; Bardelang, D. EPR Spectroscopy: A Powerful Tool to Analyze Supramolecular Host-Guest Complexes of Stable Radicals with Cucurbiturils. *Molecules* **2020**, *25*, 776; https://doi.org/10.3390/molecules25040776
- (35) Casano, G.; Poulhès, F.; Tran, T. K.; Ayhan, M. M.; Karoui, H.; Siri, D.; Gaudel-Siri, A.; Rockenbauer, A.; Jeschke, G.; Bardelang, D.; Tordo, P.; Ouari. O. High binding yet accelerated guest rotation within a cucurbit[7]uril complex. Toward paramagnetic gyroscopes and rolling nanomachines. *Nanoscale* 2015, 7, 12143–12150.
- (36) Yi, S.; Captain, B.; Ottaviani, M. F.; Kaifer, A. E. Controlling the Extent of Spin Exchange Coupling in 2,2,6,6-Tetramethylpiperidine-1-oxyl (TEMPO) Biradicals via Molecular Recognition with Cucurbit[n]uril Hosts. *Langmuir* **2011**, *27*, 5624–5632.
- (37) Moghaddam, S.; Yang, C.; Rekharsky, M.; Ko, Y. H.; Kim, K.; Inoue, Y.; Gilson, M. K. New Ultrahigh Affinity Host-Guest Complexes of Cucurbit[7]uril with Bicyclo[2.2.2]octane and Adamantane Guests: Thermodynamic Analysis and Evaluation of M2 Affinity Calculations. J. Am. Chem. Soc. 2011, 133, 3570–3581.
- (38) Mezzina E.; Cruciani F.; Pedulli G. F.; Lucarini M. Nitroxide radicals as probes for exploring the binding properties of the cucurbit[7]uril host. Chem. Eur. J. 2007, 13, 7223–7233.
- (39) Chernikova, E.; Berdnikova, D.; Fedorov, Y.; Fedorova, O.; Peregudov, A.; Isaacs, L. Self-assembly of a ternary architecture driven by cooperative Hg²⁺ ion binding between cucurbit[7]uril and crown ether macrocyclic hosts. *Chem. Commun.* **2012**, *48*, 7256–7258.
- (40) Ong, W.; Kaifer, A. E. Salt Effects on the Apparent Stability of the Cucurbit[7]uril-Methyl Viologen Inclusion Complex. *J. Org. Chem.* **2004**, *69*, 1383–1385.
- (41) Tang, H.; Fuentealba, D.; Ho Ko, Y.; Selvapalam, N.; Kim, K.; Bohne, C. Guest Binding Dynamics with Cucurbit[7]uril in the Presence of Cations. *J. Am. Chem. Soc.* **2011**, *133*, 20623–20633.
- (42) Kirilyuk, I.; Polovyanenko, D.; Semenov, S.; Grigor'ev, I.; Gerasko, O.; Fedin, V.; Bagryanskaya, E. Inclusion Complexes of Nitroxides of Pyrrolidine and Imidazoline Series with Cucurbit[7]uril. *J. Phys. Chem. B* **2010**, *114*, 1719–1728.
- (43) Ratcliffe, C. I.; Ripmeester, J. A.; Hwang, I.; Sung Jeon, W.; Kim, H.-J.; Kim, D.; Kim, H.; Selvapalam, N.; Fujita, N.; Shinkai, S.; Kim, K. Cucurbit[7]uril: A Simple Macrocyclic, pH-Triggered Hydrogelator Exhibiting Guest-Induced Stimuli-Responsive Behavior. Angew. Chem. Int. Ed. 2007, 46, 210 –213.
- (44) Bardelang, D.; Udachin, K. A.; Leek, D. M.; Margeson, J. C.; Chan, G. Cucurbit[n]urils (n = 5-8): A Comprehensive Solid State Study. *Cryst. Growth Des.* **2011**, *11*, 5598–5614.
- (45) Kim, J.; Jung, I.-S.; Kim, S.-Y.; Lee, E.; Kang, J.-K.; Sakamoto, S.; Yamaguchi, K.; Kim, K. New Cucurbituril Homologues: Syntheses, Isolation, Characterization, and X-ray Crystal Structures of Cucurbit[n]uril (n = 5, 7, and 8). *J. Am. Chem. Soc.* **2000**, *122*, 540–541.
- (46) Jeon, W. S.; Moon, K.; Park, S. H.; Chun, H.; Ko, Y. H.; Lee, J. Y.; Lee, E. S.; Samal, S.; Selvapalam, N.; Rekharsky, M. V.; Sindelar, V.; Sobransingh, D.; Inoue, Y.; Kaifer, A. E.; Kim, K. Complexation of Ferrocene Derivatives by the Cucurbit[7]uril Host: A Comparative Study of the Cucurbituril and Cyclodextrin Host Families. J. Am. Chem. Soc. 2005, 127, 12984–12989.
- (47) Hostaš, J.; Sigwalt, D.; Šekutor, M.; Ajani, H.; Dubecký, M.; Řezáč, J.; Zavalij, P. Y.; Cao, L.; Mlinarić-Majerski, K.; Isaacs, L.; Glaser, R.; Hobza, P. A Nexus between Theory and Experiment: Non-Empirical Quantum Mechanical Computational Methodology Applied to Cucurbit[n]uril·Guest Binding Interactions. Chem. Eur. J. 2016, 22, 17226–17238.

- (48) Bardelang, D.; Banaszak, K.; Karoui, H.; Rockenbauer, A.; Waite, M.; Udachin, K.; Ripmeester, J. A.; Ratcliffe, C. I.; Ouari, O.; Tordo, P. Probing Cucurbituril Assemblies in Water with TEMPO-like Nitroxides: A Trinitroxide Supraradical with Spin-Spin Interactions. J. Am. Chem. Soc. 2009, 131, 5402– 5404.
- (49) Peresypkina, E. V.; Fedin, V. P.; Maurel, V.; Grand, A.; Rey, P.; Vostrikova, K. E., Inclusion of a Nitronyl Nitroxyl Radical and Its Hydrochloride in Cucurbit[8]uril. *Chemistry – A European Journal* 2010, 16, 12481–12487.
- (50) Jayaraj, N.; Porel, M.; Ottaviani, M. F.; Maddipatla, M. V. S. N.; Modelli, A.; Da Silva, J. P.; Bhogala, B. R.; Captain, B.; Jockusch, S.; Turro, N. J.; Ramamurthy, V. Self-Aggregation of Supramolecules of Nitroxides@Cucurbit[8]uril Revealed by EPR Spectra. *Langmuir* 2009, 25, 13820–13832.
- (51) Vostrikova, K. E.; Peresypkinaa, E. V.; Drebushchak, V. A. Cucurbituril-assisted transformation of nitronyl nitroxide into imino nitroxide in the solid state. *CrystEngComm*, 2011, 13, 3241–3245.
- (52) Stoll, S.; Schweiger, A. EasySpin, a comprehensive software package for spectral simulation and analysis in EPR. J. Magn. Reson. 2006, 178, 42–55.
- (53) Spulber, M.; Schlick, S.; Villamena, F. A. Guest Inclusion in Cucurbiturils Studied by ESR and DFT: The Case of Nitroxide Radicals and Spin Adducts of DMPO and MNP. J. Phys. Chem. A 2012, 116, 8475–8483.
- (54) Livshits, V. A.; Meshkov, B. B.; Avakyan, V. G.; Titov, S. V. ESR, STESR, DFT, and MD Study of the Dynamical Structure of Cucurbituril[7]–Spin Probe Guest–Host Complexes. ACS Omega 2020, 5, 11901–11914.
- (55) Dupeyre, R.-M.; Rassat, A.; Ronzaud, J. Nitroxides. LII. Synthesis and Electron Spin Resonance Studies of N,N'-Dioxy-2,6-diazaadamantane, a Symmetrical Ground State Triplet. J. Am. Chem. Soc. 1974, 96, 6559–6568.
- (56) Eaton, S. S.; Rajca, A.; Yang, Z.; Eaton, G. R. Azaadamantyl nitroxide spin label: complexation with β-cyclodextrin and electron spin relaxation. *Free Radical Res.* 2018, 52, 319–326. DOI: 10.1080/10715762.2017.1384954
- (57) Weaver, L. H.; Matthews, B. W. Structure of bacteriophage T4 lysozyme refined at 1.7 Å resolution. J. Mol. Biol. 1987, 193, 189–199.
- (58) Feldblum, E. S.; Arkin, I. T. Strength of a bifurcated H bond. *Proc. Natl. Acad. Sci. USA* **2014**, *111*, 4085–4090.
- (59) Langen, R.; Oh, K. J.; Cascio, D.; Hubbell, W. L. Crystal structures of spin labeled T4 lysozyme mutants: implications for the interpretation of EPR spectra in terms of structure. *Biochemistry* 2000, 39, 8396–8405.
- (60) Guo, Z.; Cascio, D.; Hideg, K.; Hubbell, W. L. Structural determinants of nitroxide motion in spin-labeled proteins: solvent-exposed sites in helix B of T4 lysozyme. *Protein Sci.* 2008, 17, 228–239
- (61) Balo, A. R.; Feyrer, H.; Ernst, O. P. Toward Precise Interpretation of DEER-Based Distance Distributions: Insights from Structural Characterization of V1 Spin-Labeled Side Chains. *Biochemistry* 2016, 55, 5256–5263.
- (62) 28740983, Consentius, P.; Gohlke, U.; Loll, B.; Alings, C.; Heinemann, U.; Wahl, M. C.; Risse, T. Combining EPR spectroscopy and X-ray crystallography to elucidate the structure and dynamics of conformationally constrained spin labels in T4 lysozyme single crystals. *Phys. Chem. Chem. Phys.* 2017, 19, 20723–20734.
- (63) Guo, Z.; Cascio, D.; Hideg, K.; Kálái, T.; Hubbell, W. L. Structural determinants of nitroxide motion in spin-labeled proteins: tertiary contact and solvent-inaccessible sites in helix G of T4 lysozyme. *Protein Sci.* 2007, 16, 1069–1086.
- (64) Consentius, P.; Gohlke, U.; Loll, B.; Alings, C.; Müller, R.; Heinemann, U.; Kaupp, M.; Wahl, M.; Risse, T. Tracking Transient Conformational States of T4 Lysozyme at Room Temperature

- Combining X-ray Crystallography and Site-Directed Spin Labeling. *J. Am. Chem. Soc.* **2016**, *138*, 12868–12875.
- (65) Mchaourab H. S.; Lietzow M. A.; Hubbell W. L. Motion of spinlabeled side chains in T4 lysozyme. Correlation with protein structure and dynamics. *Biochemistry* **1996**, *35*, 7692–7704.
- (66) Hustedt, E. J.; Marinelli, F.; Stein, R. A.; Faraldo-Gómez, J. D.; Mchaourab, H. S. Confidence Analysis of DEER Data and Its Structural Interpretation with Ensemble-Biased Metadynamics. *Biophys. J.* 2019, 115, 1200–1216.
- (67) Hayashi, Y.; Puzenko, A.; Balin, I.; Ryabov, Y. E.; Feldman, Y. Relaxation Dynamics in Glycerol–Water Mixtures. 2. Mesoscopic Feature in Water Rich Mixtures. J. Phys. Chem. B 2005, 109, 9174–9177.
- (68) Popov, I.; Greenbaum, A.; Sokolov, A. P.; Feldman, Y. The puzzling first-order phase transition in water–glycerol mixtures. *Phys. Chem. Chem. Phys.* **2015**, *17*, 18063–18071.
- (69) Bordignon, E.; Nalepa, A. I.; Savitsky, A.; Braun, L.; Jeschke, G. Changes in the Microenvironment of Nitroxide Radicals around the Glass Transition Temperature. J. Phys. Chem. B 2015, 119, 13797–13806.
- (70) SAINT v. 2018.1, Bruker AXS, Madison, WI, 2018.
- (71) SADABS v. 2018.1, Bruker AXS, Madison, WI, 2018.
- (72) Sheldrick, G. M. SHELXT Integrated space-group and crystalstructure determination. *Acta Cryst. A* **2015**, *71*, 3–8.
- (73) Sheldrick, G. M. Crystal structure refinement with SHELXL. Acta Cryst. C 2015, 71, 3–8.
- (74) Kabsch, W. XDS. Acta Cryst. D 2010, 66, 125–132.
- (75) Evans, P. R. Scaling and assessment of data quality. *Acta Cryst. D* **2006**, 62, 72–82.
- (76) Evans, P. R.; Murshudov, G. N. How good are my data and what is the resolution? *Acta Cryst. D* **2013**, *69*, 1204–1214.
- (77) McCoy, A. J; Grosse-Kunstleve, R. W.; Adams, P. D.; Winn, M. D.; Storoni, L. C.; Read, R. J. Phaser crystallographic software. *J. Appl. Cryst.* 2007, 40, 658–674.
- (78) Kamenik, A. S.; Singh, I.; Lak, P.; Balius, T. E.; Liedl, K. R.; Shoichet, B. K. Energy penalties enhance flexible receptor docking in a model cavity. *Proc. Natl. Acad. Sci. USA* **2021**, *118*, e2106195118. DOI: https://doi.org/10.1073/pnas.2106195118
- (79) Liebschner, D.; Afonine, P. V.; Baker, M. L.; Bunkoczi, G.; Chen, V. B.; Croll, T. I.; Hintze, B.; Hung, L. W.; Jain, S.; McCoy, A. J.; Moriarty, N. W.; Oeffner, R. D.; Poon, B. K.; Prisant, M. G.; Read, R. J.; Richardson, J. S.; Richardson, D. C.; Sammito, M. D.; Sobolev, O. V.; Stockwell, D. H.; Terwilliger, T. C.; Urzhumtsev, A. G.; Videau, L. L.; Williams, C. J.; Adams, P. D. Macromolecular structure determination using X-rays, neutrons and electrons: recent developments in Phenix. Acta Crystallogr. D 2019, 75, 861–877.
 DOI: https://doi.org/10.1107/s2059798319011471
- (80) Schüttelkopf, A. W.; van Aalten, D. M. F. PRODRG: a tool for high-throughput crystallography of protein-ligand complexes. Acta Crystallogr. D 2004, 60, 1355–1363.
- (81) Emsley, P.; Cowtan, K. *Coot*: model-building tools for molecular graphics. *Acta Crystallogr. D* **2004**, *60*, 2126 2132.
- (82) Williams, C. J., Headd, J. J., Moriarty, N. W., Prisant, M. G., Videau, L. L., Deis, L. N., Verma, V., Keedy, D. A., Hintze, B. J., Chen, V. B., Jain, S., Lewis, S. M., Arendall, W. B. 3rd, Snoeyink, J., Adams, P. D., Lovell, S. C., Richardson, J. S., Richardson, D. C. *MolProbity*: More and better reference data for improved all-atom structure validation. *Protein Science* 2018, 27, 293–315.
- (83) Merritt, E. A. To B or not to B: a question of resolution? *Acta Crystallogr. D* **2012**, *68*, 468–477.
- (84) Winn, M. D., Ballard, C. C., Cowtan, K. D., Dodson, E. J., Emsley, P., Evans, P. R., Keegan, R. M., Krissinel, E. B., Leslie, A. G. W., McCoy, A., McNicholas, S. J., Murshudov, G. N., Pannu, N. S., Potterton, E. A., Powell, H. R., Read, R. J., Vagin, A., Wilson, K. S. Overview of the CCP4 suite and current development. *Acta. Crystallogr. D* 2011, 67, 235–242.

- (85) Matthews B. W. Structural and genetic analysis of the folding and function of T4 lysozyme. *FASEB Journal* **1996**, *10*, 35–41.
- (86) Pannier, M.; Veit, S.; Godt, A.; Jeschke, G.; Spiess, H. W. Deadtime free measurement of dipole-dipole interactions between electron spins. *J. Magn. Reason.* **2000**, *142*, 331–340.
- (87) Brandon, S.; Beth, A. H.; Hustedt, E. J. The global analysis of DEER data. *J. Magn. Reason.* **2012**, *218*, 93–104.
- (88) Stein, R. A.; Beth, A. H.; Hustedt, E. J. A Straightforward Approach to the Analysis of Double Electron-Electron Resonance Data. *Methods in Enzymology* **2015**, *563*, 531–567.

SYNOPSIS TOC (Word Style "SN_Synopsis_TOC"). If you are submitting your paper to a journal that requires a synopsis graphic and/or synopsis paragraph, see the Instructions for Authors on the journal's homepage for a description of what needs to be provided and for the size requirements of the artwork.

Insert Table of Contents artwork here

